Androgen deprivation-mediated activation of AKT is enhanced in prostate cancer with *TMPRSS2:ERG* fusion

Fen Ma[*,1], Sen Chen[*,1], Carla Calagua[1], Seiji Arai[1,2], Fang Xie[1], Olga Voznesensky[1], Larysa Poluben[1], Eva Corey[3], Changmeng Cai[1,4], Yuzhuo Wang[5], David J. Einstein[1], Mary-Ellen Taplin[6], Huihui Ye[1], Adam G. Sowalsky[1,7], Joshua W. Russo[1], Xin Yuan[1], Steven P. Balk[1]

[1]Department of Medicine and Cancer Center, Beth Israel Deaconess Medical Center, Harvard Medical School, Boston, MA 02115, USA

[2]Department of Urology, Gunma University Hospital, Maebashi, Gunma, Japan

[3]Department of Urology, University of Washington School of Medicine, Seattle, Washington, USA

[4]Center for Personalized Cancer Therapy and Department of Biology, University of Massachusetts Boston, Boston, Massachusetts, USA

[5]Vancouver Prostate Centre, University of British Columbia, Vancouver, BC, V6H 3Z6 Canada

[6]Department of Medical Oncology, Dana-Farber Cancer Institute, Harvard Medical School, Boston, MA, USA.

[7]Genitourinary Malignancies Branch, National Cancer Institute, Bethesda, MD, USA

*co-first authors

Address correspondence to Steven P. Balk, Beth Israel Deaconess Medical Center, 330 Brookline Avenue, Boston, MA 02115 email: sbalk@bidmc.harvard.edu

Abstract

The *TMPRSS2:ERG* gene fusion (*T:E* fusion) in prostate adenocarcinoma (PCa) puts ERG under the androgen receptor (AR) regulated expression of *TMPRSS2*. The *T:E* fusion is frequently associated with *PTEN* loss, and is highly correlated with decreased expression of *INPP4B*, both of which may compensate for ERG-mediated suppression of PI3K/AKT signaling. We confirmed in PCa cells and a mouse PCa model that ERG suppresses AKT activation, and that one potential mechanism is through downregulation of *IRS2*. In contrast, ERG knockdown did not increase INPP4B, suggesting its decreased expression is indirect and reflects selective pressure to suppress INPP4B function. Notably, INPP4B expression is similarly decreased in *PTEN*-intact and *PTEN*-deficient *T:E* fusion tumors, suggesting selection for a function distinct from regulation of PI3K activity. As ERG expression in *T:E* fusion tumors is AR regulated, we further assessed the extent to which AR inhibition increased AKT activity in *T:E* fusion tumors. *T:E* fusion positive versus negative PDXs had greater increases in AKT activity after castration. Moreover, in a neoadjuvant trial of AR inhibition prior to radical prostatectomy we similarly found greater increases in AKT activation in the *T:E* fusion tumors. Together these findings indicate that AKT activation may mitigate the efficacy of AR targeted therapy in *T:E* fusion PCa, and that these patients may most benefit from combination therapy targeting AR and AKT.

Introduction

The *TMPRSS2:ERG* fusion (*T:E* fusion) puts *ERG* under the androgen receptor (AR) regulated expression of *TMPRSS2*, and is an early truncal alteration found in about half of prostate adenocarcinoma (PCa) cases in men of European ancestry. It can occur through an interstitial deletion of genes located between *TMPRSS2* and *ERG* on chromosome 21, or through a genomic rearrangement that preserves the intervening genes. Some early studies had indicated that tumors with the *T:E* fusion (or possibly with *T:E* fusion associated with an interstitial deletion) were more aggressive, but further studies have not found any clear differences in prognosis or responses to therapy (1,2). The importance of ERG expression in driving PCa is supported by studies in the *T:E* fusion positive VCaP cell line, where RNAi mediated downregulation of ERG impairs cell growth and invasion (3,4). Moreover, transgenic overexpression of ERG in mouse prostate causes increased proliferation, and in combination with loss of one *PTEN* allele results in prostatic intraepithelial neoplasia (PIN) or invasive PCa in aged mice (5-8). In varying contexts ERG in PCa has been found to activate proteins/pathways including EZH2, EMT (through ZEB1, ZEB2, and ILK), Wnt signaling, NFkB, SOX9, and YAP1 (3,4,8-16). More recently, it has become clear that ERG expression has marked global effects on gene expression in PCa cells, and in particular on the AR cistrome and transcriptome, where it directly interacts with AR and functions to maintain or expand AR signaling and luminal epithelial lineage (16-23).

The requirement for *PTEN* loss to drive PCa progression in mice overexpressing ERG is consistent with an association between *T:E* fusion and *PTEN* loss in human PCa, with *T:E* being an initiating event and subsequent *PTEN* loss driving progression. One suggested basis for this association is that ERG is needed to maintain AR

functions related to luminal differentiation in the context of *PTEN* loss (17-23). Indeed, one study found that ERG overexpression in PCa from *Pten* deficient mouse prostate mitigated responses to both AR targeted therapy and combination therapy with a phosphatidylinositol 3-kinase (PI3K) inhibitor (BEZ3235), and this was associated with maintenance of AR target gene expression (19). Conversely, a recent study found that ERG could suppress PI3K signaling and subsequent AKT activation, and identified repression of insulin receptor substrate 2 (IRS2) expression as a possible mechanism (24). In this case, *PTEN* loss may be required as a secondary event to increase PI3K signaling and compensate for the repressive effects of ERG. Inositol polyphosphate-4-phosphatase type II B (INPP4B) is another phosphatase that negatively regulates PI3K signaling and has been identified as a tumor suppressor in triple negative breast cancer (25,26). Notably, analysis of TCGA data shows that *T:E* fusion in PCa is also associated with decreased expression of *INPP4B* (24). In addition to negative regulation of PI3K signaling, INPP4B has further effects on signaling pathways through regulation of endosomal trafficking of proteins including receptor tyrosine kinases (RTKs) (27-29).

Previous studies had shown that AR can suppress AKT activity by increasing expression of FKBP5, which is a scaffold for the AKT phosphatase PHLPP1 (30,31), providing a mechanism through which AR targeted therapies can increase PI3K/AKT signaling. Moreover, AR can also positively regulate expression of *INPP4B*, so that AR inhibition can further increase PI3K signaling by decreasing INPP4B (32). These stimulatory effects on PI3K may partially mitigate responses to AR inhibition, and have provided the rationale for clinical trials combining inhibition of AR and PI3K/AKT signaling (33). Notably, as ERG in *T:E* fusion PCa is driven by AR, its expression is decreased in response to AR inhibition, which may further enhance PI3K signaling and mitigate therapeutic responses. In this study we further assess ERG regulation of *IRS2*, *INPP4B*, and PI3K signaling, and test the hypothesis that AR inhibition further enhances PI3K signaling in *T:E* fusion positive PCa.

Results

T:E fusion is associated with decreased *INPP4B* expression independently of *PTEN* status

While *PTEN* loss is associated with *T:E* fusion, *PTEN* is not altered in approximately half of cases (**Figure S1A**) and its expression is not reduced in these cases where the gene is intact (**Figure 1A, S1B**). In contrast, although the *INPP4B* gene is rarely altered in primary PCa (**Figure S1A**), its mRNA levels are globally reduced in *T:E* fusion positive cases (**Figure 1B**). Consistent with this reduction, reversed phase protein analysis of PCa tumors in TCGA shows that INPP4B is the most reduced protein in *T:E* fusion positive versus negative PCa (Spearman's Correlation -0.456, p-Value 3.66e-19) (**Figure S1C**).

INPP4B dephosphorylates phosphatidylinositol 3,4-biphosphate ($PI(3,4)P_2$), which similarly to $PI(3,4,5)P_3$ mediates the binding to and activation of AKT and additional proteins with pleckstrin homology domains. Therefore, similarly to *PTEN* loss, the downregulation or loss of *INPP4B* can enhance AKT activation. However, they are not redundant. While PTEN primarily inhibits AKT activation at the plasma membrane, INPP4B targets

endosomal AKT activation and also regulates the endosomal trafficking of multiple proteins including receptor tyrosine kinases (27-29). Notably, consistent with nonredundant functions, this reduced *INPP4B* expression is independent of *PTEN* status, as it is similarly reduced in the *T:E* fusion-positive tumors whether *PTEN* is lost or intact (**Figure 1C**). Moreover, independent of *T:E* fusion status, there is a positive correlation between *PTEN* and *INPP4B* expression (**Figure 1D**). Finally, consistent with a previous study (24), *IRS2* expression is lower in *T:E* fusion positive tumors (**Figure 1E**), although this decrease is not as marked as the decrease in *INPP4B*.

ERG suppresses PI3K signaling in PCA cells in vitro

To directly assess effects of ERG on PI3K signaling and on regulation of *IRS2* and *INPP4B*, we used RNAi to decrease expression of ERG in *T:E* fusion-positive VCaP PCa cells. Consistent with a previous study (24), shRNA-mediated suppression of ERG increased PI3K signaling based on increased AKT phosphorylation at both S308 and S473, and increased S6 phosphorylation (**Figure 2A**). There was also a small increase in ERK phosphorylation. Acute suppression of ERG with siRNA similarly increased AKT and S6 phosphorylation (**Figure 2B**). Conversely, we assessed the effects of inducing ERG expression in *T:E* fusion-negative LNCaP PCa cells. For this we generated a tet-operator (tetO) regulated vector (pTET-Splice) expressing N-terminal HA-tagged ERG, using human ERG with deletion of amino acids 1-39 to mimic the product generated from the most common *T:E* fusion (pTET-ERG) (**Figure S2A, B**). This was stably transfected into LNCaP cells expressing pcDNA6/TR for doxycycline (DOX)-regulated expression. The LNCaP cells are PTEN deficient and hence have high basal PI3K/AKT signaling (**Figure 2C**). DOX-mediated induction of ERG caused a modest decrease in phosphorylation of AKT and S6, with a greater decrease in ERK phosphorylation. These results support the conclusion that ERG suppresses PI3K signaling. Notably, the suppression of ERK as well as AKT is consistent with decreased IRS2, which can mediate RTK signaling to both pathways.

ERG suppresses IRS2 directly and INPP4B indirectly

We next examined effects of ERG siRNA on IRS2 and INPP4B. Consistent with a previous report (24), ERG knockdown increased the expression of IRS2 protein (**Figure 2D**). In contrast, there was not a clear increase in INPP4B protein. RNA-seq analysis confirmed a ~2.5-fold rise in IRS2 mRNA upon ERG siRNA treatment, whereas INPP4B was not changed. Analysis of available ERG ChIP-seq data showed in VCaP cells showed an ERG binding site at the promoter of *IRS2*, but not *INPP4B*, further indicating that ERG directly regulates IRS2 and not INPP4B (**Figure S3A, B**). Notably, AR ChIP-seq shows that this ERG binding site overlaps a broad AR binding site present in VCaP cells, but not in *T:E* negative LNCaP cells (**Figure S3A**). This result is consistent with previous results showing that ERG opens cryptic AR binding sites in many genes, so these come under joint ERG and AR regulation (16). Interestingly, although ERG knockdown increases IRS2 mRNA, it did not increase H3K27Ac at the *IRS2* promoter, suggesting ERG is repressing through a mechanism distinct from modulation of histone acetylation.

To assess more broadly the effects of ERG knockdown we used gene set enrichment analysis (GSEA). PI3K-AKT-MTOR signaling was only modestly increased in ERG knockdown cells (**Figure S4A,B**), while the most enriched gene set after ERG knockdown was Androgen Response followed by Fatty Acid Metabolism (which may be androgen-regulated) (**Figure S4A, C, D**). This result is somewhat surprising as ERG can maintain or expand AR signaling in the setting of *PTEN* loss, and may reflect that VCaP is *PTEN* intact. Conversely, Hallmark gene sets including MYC targets and E2F targets were markedly decreased in response to ERG knockdown (**Figure S4A, D**), consistent with an oncogenic function of ERG in these cells. Together these results support the conclusion that ERG directly suppresses IRS2 expression. In contrast, these results also indicate that the decreased expression of INPP4B in *T:E* fusion tumors is not direct, and that it is an adaptation that is selected, at least in part, to compensate for suppressive effects of ERG on PI3K signaling, and potentially ERK signaling.

AKT activation is inversely associated with ERG expression in mouse model

We next used a mouse model to assess ERG function in an in vivo context. We used the insert from the pTET-ERG vector to generate transgenic mice expressing HA-tagged human ERG (amino acids 1-39 deleted) under the control of the tetracycline operator. We had previously developed transgenic mice with a probasin-driven reverse tetracycline transactivator (rtTA, tet-on) that can drive prostate specific expression of tetracycline operator-driven transgenes (34). These mice were crossed with the pTET-ERG transgenic mice to obtain DOX-stimulated expression of ERG in the prostate. We initially sacrificed a small cohort of mice at ~4-5 months after DOX induction, and isolated protein from each lobe. By immunoblotting we found ERG expression in the ventral lobes, which we confirmed by qRT-PCR (**Figure S5A**). By IHC we further confirmed DOX-driven ERG expression in ventral prostate (**Figure S5B**), and in two pTET-ERG lines confirmed that expression was dependent on the rtTA (**Figure S5C**). Consistent with previous studies showing a modest effect of ERG overexpression in mouse prostate (5,6), induction of ERG for as long as 16 months caused only mild hyperplasia (**Figure S4D**).

Next, crossed these mice onto a *Pten* haploinsufficient background (*Pten*$^{-/+}$) (5). In these mice we then induced ERG expression by feeding mice with both DOX food and water to further increase ERG expression (**Figure S6A, B**). We identified areas of PCa after ~11 months of DOX induction (**Figure 3A**). Notably, ERG expression was heterogeneous, with much lower ERG expression in the areas with invasive tumor (**Figure 3B**). Moreover, in those tumor areas with low ERG, we found elevated expression of pAKT(473), pS6(S235,236), and to a lesser extent pERK, reflecting activation of the PI3K/AKT pathway (**Figure 3C**). These observations were consistent with ERG suppression of PI3K/AKT signaling. The decrease in ERG in these areas may be due in part to a decrease in AR, which is driving the rtTA in these mice (**Figure S7A**). Expression of another AR-driven gene, *Tmprss2*, was also decreased in these tumor areas with low ERG (**Figure S7B**). These findings indicate that while ERG is oncogenic, higher levels may be tumor suppressive, possibly due to suppression of PI3K/AKT signaling.

ERG-regulated genes in probasin-rtTA; tetO-ERG; *Pten*$^{-/+}$ mice

To identify ERG-regulated genes that may be contributing to PCa development in this model, we carried out time course experiments with both short-term ERG induction and long term induction plus short term DOX withdrawal in the probasin-rtTA; tetO-ERG; *Pten*$^{-/+}$ (*ERG;Pten*$^{+/-}$) mice. For the short-term induction, mice were treated with DOX or vehicle for 3 or 6 days. Ventral prostate epithelium was then laser capture microdissected and transcriptome profiles were obtained using Affymetrix microarrays. The level of ERG induction based on the microarrays was similar at 3 and 6 days (~25% increase), so expression data from both days were pooled. There were 5 Hallmark gene sets that were significantly (FDR <0.25) increased and 16 decreased (**Figure S8A**). The MTORC1 Signaling and PI3K AKT MTORC Signaling were amongst the highly suppressed gene sets (NES -3.34 and -2.64 respectively) (**Figure S8B, C**). Notably, this suppression could not be attributed to IRS2, as it was not decreased by ERG induction (ratio induced/uninduced ~1.18). INPP4B was increased (ratio induced/uninduced ~1.16), indicating it may acutely contribute to decreased PI3K signaling in these mice.

Interestingly, the most altered gene involved in phosphatidylinositol metabolism was PIKFYVE (phosphoinositide kinase) (ratio induced/uninduced 0.71). This kinase phosphorylates the D-5 position in phosphatidylinositol and phosphatidylinositol-3-phosphate on endosomes, the latter generated by INPP4B, to promote lysosomal targeting. The second most altered gene in phosphatidylinositol metabolism was phosphoinositide-3-kinase regulatory subunit 3 (PIK3R3, ratio induced/uninduced 0.74), which may contribute directly to a decrease in PI3K activity in these mice. Analysis of TCGA PCa data show that PIK3R3 is also significantly decreased in *T:E* fusion tumors (**Figure S8D**), indicating this may also contribute to ERG-mediated suppression of PI3K signaling in patients.

We next used RNA-seq to assess the effects of discontinuing DOX in mice with established tumors. There were no Hallmark gene sets altered at FDR <0.25. Nonetheless, IRS2 was ~4-fold higher in tumors after DOX discontinuation, consistent with it being suppressed by ERG in the established tumors. Levels of INPP4B prior to and after DOX discontinuation were too low for reliable assessment. Interestingly, the lncRNA H19 was the most increased transcript in the DOX induced tumors versus levels after DOX withdrawal (**Figure 4A**). H19 was also increased by short-term DOX induction (although only about 2-fold versus the >100-fold increase in the long-term DOX induced tumor samples) (not shown), indicating that ERG is inducing H19. Notably, *H19* and *IGF2* are co-regulated in human and mouse by genomic imprinting through methylation at the locus between *H19* and *IGF2*, and we also observed increased IGF2 in the DOX-induced tumors versus the samples after DOX withdrawal (**Figure 4A**). Marked ERG-mediated increases in IGF2 and H19 mRNA were also observed in a previous independent study using stable probasin-ERG transgenic mice, but the significance of this increase with respect to decreased PI3K/AKT signaling is not clear (13) (**Figure 4B**).

While H19 appears to be a major target of ERG in mouse, analysis of gene expression data in human primary PCa shows that H19 is instead decreased in *T:E* fusion positive tumors (**Figure 4C**). Interestingly, analyzing *T:E* fusion-positive and *T:E* fusion-negative tumors separately we find that H19 expression is positively correlated with ERG in *T:E* negative (but not positive) tumors, but the significance of this association is not clear (**Figure 4D, E**). Together these findings indicate that H19 is a major transcriptional target of ERG in this mouse PCa model, but not in human PCa. Overall these observations support the conclusion that ERG is repressing PI3K/AKT signaling in this mouse PCa model and in human PCa, although some distinct mechanisms may be involved.

Castration enhances AKT activation in *T:E* fusion positive PDX models

As expression of ERG in *T:E* fusion positive tumors is driven by AR, it is markedly decreased in response to AR targeted therapies. Therefore, we next assessed the extent to which castration increases PI3K/AKT signaling in *T:E* fusion positive tumors. A series of PDXs were established in male *scid* mice and analyzed prior to castration and at 1-3 weeks post-castration. In the *T:E* fusion positive (and *PTEN* deficient) BIDPC4 PDX, castration decreased ERG (as expected) and caused a marked increase in phosphorylation of AKT and S6 (**Figure 5A**). To explore the role of AKT activity in this model, we generated short-term ex vivo cultures from BIDPC4 PDX cells. These cultures were treated with an AKT inhibitor (ipatasertib) in either medium containing fetal bovine serum (FBS) or androgen-depleted charcoal-stripped serum (CSS). Notably, cells in the CSS medium showed heightened sensitivity to AKT inhibition (**Figure 5B**). A similar effect was observed with a second AKT inhibitor, MK2206 (**Figure 5C**).

A similar marked increase in AKT and S6 phosphorylation was observed after castration in the *T:E* fusion-positive (also *PTEN* deficient) LuCaP 35 PDX (**Figure 6A**). Both BIDPC4 and LuCaP 35 were derived from metastases in men with CRPC. Therefore, we also examined a series of PDXs derived from primary PCa in men who were not previously treated (35). In the *T:E* fusion positive PDX LTL310 we found an increase in AKT phosphorylation at 3 weeks after castration and in the subsequent castration-resistant tumors, although it was modest compared to those above in BIDPC4 and LuCaP 35, and there was no clear increase in S6 phosphorylation (**Figure 6B**). We did not find an increase in AKT or S6 phosphorylation in a second *T:E* fusion PDX derived from untreated primary PCa (LTL313B, not shown). Finally, we did not observe increased phosphorylation of AKT or S6 after castration in a series of *T:E* fusion negative PDXs including LTL607 (**Figure 6C**), LTL508 and LTL484 (**Figure S9A, B**) or LTL573 and LTL651 (not shown).

AR signaling inhibition enhances AKT activation in *T:E* fusion positive clinical samples

We next examined samples from a clinical trial of neoadjuvant leuprolide, abiraterone, and apalutamide administered for 24 weeks prior to radical prostatectomy (RP) in men with high-risk primary PCa (NCT02903368) (36). ERG IHC on diagnostic biopsies was used to identify cases that were *T:E* fusion positive versus negative.

Diagnostic core biopsies and corresponding RP specimens containing residual tumor in the *T:E* positive and *T:E* negative cases were then stained for phospho-AKT (**Figure 6A**). Notably, phospho-AKT staining was variable in the biopsies. This may reflect factors including *PTEN* loss, which is more common in *T:E* fusion positive tumors. Therefore, to take into consideration factors other than ERG that may influence PI3K signaling, we quantified the difference in phospho-AKT staining between the biopsies and RP specimens for each case. Staining in the RP specimens was greater than in the biopsies in over half of the *T:E* positive cases versus only 2 of the *T:E* negative cases (**Figure 6B**), and this increase in the *T:E* fusion positive versus negative residual tumors was significant (**Figure 6C**).

Discussion

T:E fusion is frequently associated with *PTEN* loss and is strongly correlated with decreased *INPP4B* expression, which together may compensate for an ERG-mediated suppression of PI3K signaling. Our finding that ERG knockdown enhances PI3K signaling in *T:E* fusion positive VCaP cells supports this conclusion and is consistent with results in a previous study (24). Also consistent with this previous study, we found that ERG knockdown in VCaP cells increased IRS2, supporting ERG repression of IRS2 as a mechanism contributing to ERG suppression of PI3K signaling. In contrast, despite the strong negative correlation between ERG and INPP4B levels in clinical samples, ERG knockdown did not increase INPP4B mRNA or protein, suggesting the decreased expression of INPP4B is indirect and reflects selective pressure to decrease INPP4B function. Results in mice with DOX-regulated induction of ERG further support the conclusion that ERG suppresses PI3K signaling, although mechanisms driving this decrease and subsequent adaptations in mouse may be distinct.

Significantly, INPP4B expression is broadly decreased in *T:E* fusion positive PCa, including in cases with genomic *PTEN* loss, suggesting nonredundant functions. Indeed, PTEN regulates AKT activation primarily by targeting $P(3,4,5)P_3$ at the plasma membrane, although it may in some settings also target $P(3,4)P_2$ (37). In contrast, INPP4B-mediated dephosphorylation of $PI(3,4)P_2$ primarily regulates AKT activation intracellularly, with one study indicating that it selectively regulates the AKT2 isoform (28). Moreover, the PI(3)P it generates on endosomal membranes can enhance lysosomal targeting of signaling proteins including EGFR and GSK3β to downregulate receptor tyrosine kinase signaling and to enhance Wnt signaling, respectively (27,38,39). To the extent that *T:E* fusion tumors need to compensate for decreased IRS2, this former increase in receptor tyrosine kinase signaling may be an important factor driving selection for decreased INPP4B. Further studies are needed to address the extent to which loss of these or other INPP4B functions drive selection for its downregulation in *T:E* fusion positive PCa, and whether this results in novel therapeutic vulnerabilities.

Previous studies have shown that AR-targeted therapies can increase PI3K signaling through mechanisms including downregulation of FKBP5 and of INPP4B (30-32). As ERG is AR regulated in *T:E* fusion positive tumors, we hypothesized that AR inhibition would in particular enhance AKT activation in these tumors. Indeed, we found

that AKT activity was increased after castration in three *T:E* fusion positive PDX models, but this was not observed in *T:E* negative PDXs. Moreover, in a neoadjuvant trial of AR inhibition for 24 weeks prior to radical prostatectomy, we found greater increases in AKT activity after treatment in the *T:E* fusion positive tumors. Based on these findings, we suggest that increased AKT activity due to decreased ERG mitigates the efficacy of AR-targeted therapies to a greater extent in *T:E* fusion PCa, and that men with *T:E* fusion-positive tumors may most benefit from the addition of an AKT inhibitor to AR targeted therapy.

Notably, results of a phase 3 trial of abiraterone combined with an AKT inhibitor (ipatasertib) in CRPC indicated that there was a benefit in men with *PTEN-deficient* tumors (33). As *PTEN* loss is associated with *T:E* fusion, it is possible that some of this benefit may also reflect *T:E* fusion. Moreover, we suggest that this benefit of adding an AKT inhibitor may be greater in men with castration-sensitive PCa who are initiating AR targeted therapy. Finally, we suggest that *T:E* fusion tumors may have additional vulnerabilities, including those related to INPP4B downregulation, that may be exploited therapeutically.

Methods

Cell lines and reagents

LNCaP and VCaP cells were obtained from ATCC and cultured in RPMI-1640/10% FBS or DMEM/10% FBS, respectively. Cells were used within 6 months of thawing, and were tested negative for Mycoplasma. siRNA targeting ERG and control SiCtrl were from Dharmacon (Thermo Fisher). shRNA plasmids targeting ERG and controls were from Santa Cruz. Transfections were performed using Lipofectamine 2000 (Invitrogen) according to manufacturer instructions. The pTET-ERG plasmid was made by inserting N-terminal HA-tagged ERG (with deletion of amino acids 1-39) into the tet-operator (tetO) regulated vector pTET-Splice (Invitrogen). LNCaP cells with DOX inducible ERG were then generated by transfecting the pTET-ERG vector into a LNCAP clone carrying pcDNA6/TR, followed by selection.

RNA interference

ERG knockdown were performed in VCaP cells. Briefly, VCaP cells were transfected with 20, 40 and 60 nmol/L ON-TARGETplus siRNAs (Dharmacon) with Lipofectamine RNAiMAX (Thermo Fisher Scientific, 13778–075). At 48 hours after transfection, cells were harvested for protein purification and RNA purification.

RNA isolation and qRT-PCR

Total RNA was isolated with the RNeasy Mini Plus Kit (Qiagen, #74134). RNA purification was directly performed from 2D cultured cells. For RNA isolation from tissues, homogenization were performed using a tissue ruptor(Qiagen, cat No. 9002755). qRT-PCR was performed using standard SYBR Green reagents from the StepOnePlus Real-Time PCR system (Thermo Fisher Scientific, #11780200) or TaqMan One-Step RT-

PCR reagents (Thermo Fisher Scientific, #4444434). Target mRNA expression was quantified using the ΔΔCt method and normalized to GAPDH expression.

Animal Study Compliance

All animal studies were approved by the Beth Israel Deaconess Medical Center (BIDMC) Institutional Animal Care and Use Committee (IACUC). All procedures were approved by the BIDMC IACUC and conformed to the NIH guidelines.

Transgenic mice

The tetO regulated HA-ERG was excised from the pTET-ERG vector and used for pronuclear microinjection in FVB mice (BIDMC Transgenic Facility). Founder lines determined by genotyping were then bred with transgenic mice we generated previously expressing a probasin-driven reverse tetracycline transactivator (rtTA, tet-on), which we showed could drive prostate specific expression of tetracycline operator-driven transgenes (34). Transgene expression was induced by feeding a rodent diet containing doxycycline chow (0.625g/kg, Harlan Tekland, Indianapolis, IN) alone or with drinking water containing 1g/L DOX in 1% dextrose. *Pten* deficient mice on a C57Bl/6J background were generously provided by Dr. Pandolfi. Prostates were dissected and snap-frozen for RNA/protein extraction or formalin-fixed for paraffin embedding.

PDX tumors

The BIDPC4 PDX was generated from an omental metastasis in a patient with *T:E* fusion CRPC. Exome sequencing shows in addition the following: *AR* amplification, *PIK3CA* H419_L422del, *PTEN* loss, *MYC* amplification, *FAS* loss, *TP53* G245S. LuCaP 35 and the series of LTL primary PCA PDXs were described previously (35,40). Male 5–6 weeks old ICR SCID mice were purchased from Taconic and housed in the Animal Research Facility at Beth Israel Deaconess Medical Center (BIDMC, Boston, MA). Patient-derived xenografts (PDX) were initially established by inoculating human biopsies both subcutaneously and by renal graft with 50% Matrigel. Upon successful establishment, tumors were harvested and minced into 1-2mm^3 tumor bits and cryopreserved. Portions of the tumors were then further expanded subcutaneously in mice, all materials in this study are early passages.

Ex vivo culture establishment

The ex-vivo cultures were generated from PDXs by culturing in standard DMEM medium with 10% FBS or 10% Charcoal-Stripped Serum(CCS) and 5% Matrigel, without further additives. Briefly, the tumor was excised from subcutaneous xenografts around 500 mm^3, rinsed with DMEM(gentamicin 50ug/ml), and washed with DMEM and minced into 1-2mm^3 tumor bits. The tumor bits were digested with collagenase/dispase (Millipore Sigma, #10269638001 and #11097113001, respectively) at 37°C for 30 minutes. The digestion was then stopped by adding medium with 10% FBS, and the slurry went through 100uM filter to remove big chunks. The tumor cells were collected by centrifugation. Resuspended cell pellets were then seeded in DMEM either with 10% FBS or

10% CCS and containing 5% (v/v) Matrigel (CORNING, catalog no. 356230), and plated at 0.8~1 × 104 cells per well in 96-well plate.

CellTiter-Glo luminescent cell viability assay

Ex-vivo cultures generated from PC4 PDX were cultured with DMEM plus either 10% FBS or 10%CCS and 5% Matrigel in 96-well plates. Cells were treated with nine doses of pan AKT inhibitors, serial diluting from 20uM with a dilution factor of 2. Six replicates were set up for each dose. CellTiter-Glo luminescent cell viability assay (Promega, G7571) was performed after 7 days of treatment according to the manufacturer's protocol. The killing curve was plotted based on the readout, which is normalized to the average luminescent signal of DMSO under the respective conditions (Supplementary Fig. S9). Two independent AKT inhibitors were used, including MK2206(MedchemExpress, Cat No. HY-10358) and ipatasertib(MedChemExpress, Cat /no. HY-15186. Experiments were repeated at least three times, and representative results were shown.

Immunoblotting

Proteins were extracted in RIPA buffer (50 mM Tris pH 8.0 with 1% TritonX-100, 0.5% deoxycholate, 0.1% SDS) containing Pierce protease inhibitor and phosphatase inhibitor cocktails (Thermo Scientific), with addition of 1 mM sodium orthovanadate. Protein extracts were immunoblotted with antibodies against AKT pS473 (Cell Signaling rabbit mAb #4058, 1:1000) or pT308 (Cell Signaling rabbit mAb #2965, 1:1000), S6 pS235,236 (Cell Signaling #2211, 1:000), ERK pT202,Y204 (Cell Signaling rabbit mAb #4858, 1:1000), AR (mAb 441, Abcam #ab9474, 1:1000), ERG (Cell Signaling rabbit mAb #97249, 1:1000), Vinculin (Cell Signaling rabbit mAb #13901, 1:1000), PRAS40 (Cell Signaling rabbit mAb #13175, 1:1000), INPP4B (Cell Signaling rabbit mAb #14543, 1:1000), IRS2 (Cell Signaling rabbit mAb #4502, 1:1000), and HA (Covance rabbit polyclonal #PRB-101C, 1:1000).

Immunohistochemistry

For immunostaining, slides were depariffinized, rehydrated, heated in boiling 10 mmol/L citrate buffer (pH 6.2) for 30 minutes, and blocked using 5% goat serum. Primary antibodies were anti-pAKT (pS473, Cell Signaling rabbit mB #4058, 1:200), anti-HA (Cell Signaling rabbit mAb #3724, 1:200), anti-pS6 (S240/244, Cell Signaling, #2211, 1:200), anti-AR (Upstate rabbit polyclonal #06-680, 1:100), TMPRSS2 (Cell Signaling rabbit mAb #84382), and anti-ERG (Abcam rabbit mAb EPR3864 #ab92513, 1:100) in 1% BSA. These were incubated overnight at 4ºC, followed by biotinylated secondary antibody and streptavidin-HRP (1:400, Vector). Slides were developed with 3,3-diaminobenzidine (DAB) and counterstained with hematoxylin. For the NCT02903368 clinical trial we analyzed individual pretreatment core biopsies and a series of TMAs containing residual tumor from the post therapy radical prostatectomies. The TMAs contained 3 mm punches taken from 2-4 representative tumor foci based on histology. The *T:E* fusion status of the cases was determined by immunohistochemistry using an ERG antibody (2). Staining for pAKT was scored based on the fraction of positive cells, with a score of 0 for

none, 1 for 1-5%, 2 for 5-25%, 3 for 25-50%, and 4 for >50%. The focus on the TMA from each case with the highest score was used for comparison with the pretreatment core biopsy. The scoring was carried out independently by two investigators who were blinded to ERG status.

Transcriptome analyses

Total RNA was isolated using the RNeasy Plus Kit (Qiagen) following the manufacturer's instructions. RNA from mouse prostate prior to and post DOX induction was analyzed by hybridization on Affymetrix Mouse Gene 1.0 ST arrays. For RNA-seq, mRNA libraries were generated using the Illumina TruSeq stranded mRNA sample kit. Raw reads were analyzed using a pipeline for RNA-seq analysis - Visualization Pipeline for RNA-seq analysis (VIPER) based on workflow management system Snakemake (https://github.com/hanfeisun/viper-rnaseq). The read alignment to the hg19 reference genome was performed using STAR aligner (2.7.0f) with default parameters. Gene expression (FPKM values) was quantitated with Cufflinks (v2.2.1). After ranking according to differential expression, Gene Set Enrichment Analysis (GSEA) was performed to search for enrichment across the Molecular Signatures Database using GSEA webtool(https://www.gsea-msigdb.org/gsea/index.jsp). Analysis of public RNA-seq data from TCGA was done in cBioPortal (41,42).

Chromatin immunoprecipitation sequencing analysis

Chromatin immunoprecipitation sequencing (ChIP-seq) data for ERG, H3K27Ac, H3K4me3, H3K4me1 were obtained from following list. ChIP-seq profiles of ERG and multiple histone modifiers flanking the IRS2 gene were demonstrated using IGV reference to Hg38.

Sample name	**GEO**
VCaP NTC DHT ERG	GSM2086309
VCaP SICTL H3K27AC CHIP-SEQ, REP2	GSM2537220
VCaP SIERG H3K27AC CHIP-SEQ, REP2	GSM2537223
VCaP_Ethl_H3K4me3	GSM353603
VCaP_regular_medium_H3K4me1	GSM353631
LNCaP_ERG	GSM353648
H3K27AC LNCaP-DHT	GSM1249447
LNCaP_regular_medium_H3K4me3	GSM353626
LNCaP_regular_medium_H3K4me1	GSM353634

Statistical analysis

GraphPad Prism 9 Software (GraphPad Software Inc.) was used for all statistical analysis unless otherwise specified. The significance of difference between two groups was determined by two-tailed Student t test. Both Pearson and Spearman correlation were used for correlation analysis. Statistical significance was accepted at

$P < 0.05$. Nonlinear regression curve fitting with a variable slope model was applied to assess the dose-response of AKT inhibitors, and IC50 generated for each inhibitor under both FBS and CCS conditions.

Acknowledgments

This work was supported by NIH R01 CA168393 and CA272934-01 (SPB, XY), NIH P01 CA163227 (SPB, EC), NIH P50 CA272390 (SPB, MET), NIH U54 CA156734 (SPB, CC), Department of Defense PCRP Idea Development Award W81XWH-20-1-0925 (FM, SPB), Department of Defense PCRP Idea Development Award W81XWH-15-1-0151 (XY), Prostate Cancer Foundation Challenge Awards (SPB, MET, EC), a Research Fellowship from Gunma University Hospital (SA), and the Intramural Research Program of the National Cancer Institute (AGS). We thank Drs. Alex Toker, John Clohessy, and Johann de Bono for helpful discussions.

Conflicts of Interest

EC served as a paid consultant to DotQuant, and received Institutional sponsored research funding unrelated to this work from AbbVie, Gilead, Sanofi, Zenith Epigenetics, Bayer Pharmaceuticals, Forma Therapeutics, Genentech, GSK, Janssen Research, Kronos Bio, Foghorn Therapeutics, K36, and MacroGenics. The other authors declare no conflicts of interest.

References Cited

1. Gopalan A, Leversha MA, Satagopan JM, Zhou Q, Al-Ahmadie HA, Fine SW*, et al.* TMPRSS2-ERG gene fusion is not associated with outcome in patients treated by prostatectomy. Cancer Res **2009**;69(4):1400-6 doi 10.1158/0008-5472.CAN-08-2467.

2. Pettersson A, Graff RE, Bauer SR, Pitt MJ, Lis RT, Stack EC*, et al.* The TMPRSS2:ERG rearrangement, ERG expression, and prostate cancer outcomes: a cohort study and meta-analysis. Cancer Epidemiol Biomarkers Prev **2012**;21(9):1497-509 doi 10.1158/1055-9965.EPI-12-0042.

3. Tomlins SA, Laxman B, Varambally S, Cao X, Yu J, Helgeson BE*, et al.* Role of the TMPRSS2-ERG gene fusion in prostate cancer. Neoplasia **2008**;10(2):177-88.

4. Wang J, Cai Y, Yu W, Ren C, Spencer DM, Ittmann M. Pleiotropic biological activities of alternatively spliced TMPRSS2/ERG fusion gene transcripts. Cancer Res **2008**;68(20):8516-24 doi 10.1158/0008-5472.CAN-08-1147.

5. Carver BS, Tran J, Gopalan A, Chen Z, Shaikh S, Carracedo A*, et al.* Aberrant ERG expression cooperates with loss of PTEN to promote cancer progression in the prostate. Nat Genet **2009**;41(5):619-24 doi 10.1038/ng.370.

6. King JC, Xu J, Wongvipat J, Hieronymus H, Carver BS, Leung DH*, et al.* Cooperativity of TMPRSS2-ERG with PI3-kinase pathway activation in prostate oncogenesis. Nat Genet **2009**;41(5):524-6 doi 10.1038/ng.371.

7. Zong Y, Xin L, Goldstein AS, Lawson DA, Teitell MA, Witte ON. ETS family transcription factors collaborate with alternative signaling pathways to induce carcinoma from adult murine prostate cells. Proc Natl Acad Sci U S A **2009**;106(30):12465-70 doi 10.1073/pnas.0905931106.

8. Klezovitch O, Risk M, Coleman I, Lucas JM, Null M, True LD*, et al.* A causal role for ERG in neoplastic transformation of prostate epithelium. Proc Natl Acad Sci U S A **2008**;105(6):2105-10 doi 10.1073/pnas.0711711105.

9. Yu J, Yu J, Mani RS, Cao Q, Brenner CJ, Cao X*, et al.* An integrated network of androgen receptor, polycomb, and TMPRSS2-ERG gene fusions in prostate cancer progression. Cancer Cell **2010**;17(5):443-54 doi 10.1016/j.ccr.2010.03.018.

10. Kunderfranco P, Mello-Grand M, Cangemi R, Pellini S, Mensah A, Albertini V*, et al.* ETS transcription factors control transcription of EZH2 and epigenetic silencing of the tumor suppressor gene Nkx3.1 in prostate cancer. PLoS One **2010**;5(5):e10547 doi 10.1371/journal.pone.0010547.

11. Gupta S, Iljin K, Sara H, Mpindi JP, Mirtti T, Vainio P*, et al.* FZD4 as a mediator of ERG oncogene-induced WNT signaling and epithelial-to-mesenchymal transition in human prostate cancer cells. Cancer Res **2010**;70(17):6735-45 doi 10.1158/0008-5472.CAN-10-0244.

12. Wang J, Cai Y, Shao LJ, Siddiqui J, Palanisamy N, Li R*, et al.* Activation of NF-{kappa}B by TMPRSS2/ERG Fusion Isoforms through Toll-Like Receptor-4. Cancer Res **2011**;71(4):1325-33 doi 10.1158/0008-5472.CAN-10-2210.

13. Nguyen LT, Tretiakova MS, Silvis MR, Lucas J, Klezovitch O, Coleman I*, et al.* ERG Activates the YAP1 Transcriptional Program and Induces the Development of Age-Related Prostate Tumors. Cancer Cell **2015**;27(6):797-808 doi 10.1016/j.ccell.2015.05.005.

14. Leshem O, Madar S, Kogan-Sakin I, Kamer I, Goldstein I, Brosh R*, et al.* TMPRSS2/ERG promotes epithelial to mesenchymal transition through the ZEB1/ZEB2 axis in a prostate cancer model. PLoS One **2011**;6(7):e21650 doi 10.1371/journal.pone.0021650.

15. Becker-Santos DD, Guo Y, Ghaffari M, Vickers ED, Lehman M, Altamirano-Dimas M*, et al.* Integrin-linked kinase as a target for ERG-mediated invasive properties in prostate cancer models. Carcinogenesis **2012**;33(12):2558-67 doi 10.1093/carcin/bgs285.

16. Cai C, Wang H, He HH, Chen S, He L, Ma F*, et al.* ERG induces androgen receptor-mediated regulation of SOX9 in prostate cancer. J Clin Invest **2013**;123(3):1109-22 doi 10.1172/JCI66666.

17. Blee AM, He Y, Yang Y, Ye Z, Yan Y, Pan Y*, et al.* TMPRSS2-ERG Controls Luminal Epithelial Lineage and Antiandrogen Sensitivity in PTEN and TP53-Mutated Prostate Cancer. Clin Cancer Res **2018**;24(18):4551-65 doi 10.1158/1078-0432.CCR-18-0653.

18. Li F, Yuan Q, Di W, Xia X, Liu Z, Mao N*, et al.* ERG orchestrates chromatin interactions to drive prostate cell fate reprogramming. J Clin Invest **2020** doi 10.1172/JCI137967.

19. Mao N, Gao D, Hu W, Hieronymus H, Wang S, Lee YS*, et al.* Aberrant Expression of ERG Promotes Resistance to Combined PI3K and AR Pathway Inhibition through Maintenance of AR Target Genes. Mol Cancer Ther **2019**;18(9):1577-86 doi 10.1158/1535-7163.MCT-18-1386.

20. Wasmuth EV, Hoover EA, Antar A, Klinge S, Chen Y, Sawyers CL. Modulation of androgen receptor DNA binding activity through direct interaction with the ETS transcription factor ERG. Proc Natl Acad Sci U S A **2020**;117(15):8584-92 doi 10.1073/pnas.1922159117.

21. Shah N, Kesten N, Font-Tello A, Chang MEK, Vadhi R, Lim K*, et al.* ERG-mediated coregulator complex formation maintains androgen receptor signaling in prostate cancer. Cancer Res **2020** doi 10.1158/0008-5472.CAN-20-2044.

22. Chen Y, Chi P, Rockowitz S, Iaquinta PJ, Shamu T, Shukla S*, et al.* ETS factors reprogram the androgen receptor cistrome and prime prostate tumorigenesis in response to PTEN loss. Nat Med **2013**;19(8):1023-9 doi 10.1038/nm.3216.

23. Wasmuth EV, Broeck AV, LaClair JR, Hoover EA, Lawrence KE, Paknejad N*, et al.* Allosteric interactions prime androgen receptor dimerization and activation. Mol Cell **2022**;82(11):2021-31 e5 doi 10.1016/j.molcel.2022.03.035.

24. Mao N, Gao D, Hu W, Gadal S, Hieronymus H, Wang S*, et al.* Oncogenic ERG Represses PI3K Signaling through Downregulation of IRS2. Cancer Res **2020**;80(7):1428-37 doi 10.1158/0008-5472.CAN-19-1394.

25. Gewinner C, Wang ZC, Richardson A, Teruya-Feldstein J, Etemadmoghadam D, Bowtell D*, et al.* Evidence that inositol polyphosphate 4-phosphatase type II is a tumor suppressor that inhibits PI3K signaling. Cancer Cell **2009**;16(2):115-25 doi 10.1016/j.ccr.2009.06.006.

26. Fedele CG, Ooms LM, Ho M, Vieusseux J, O'Toole SA, Millar EK*, et al.* Inositol polyphosphate 4-phosphatase II regulates PI3K/Akt signaling and is lost in human basal-like breast cancers. Proc Natl Acad Sci U S A **2010**;107(51):22231-6 doi 10.1073/pnas.1015245107.

27. Liu H, Paddock MN, Wang H, Murphy CJ, Geck RC, Navarro AJ*, et al.* The INPP4B Tumor Suppressor Modulates EGFR Trafficking and Promotes Triple-Negative Breast Cancer. Cancer Discov **2020**;10(8):1226-39 doi 10.1158/2159-8290.CD-19-1262.

28. Li Chew C, Lunardi A, Gulluni F, Ruan DT, Chen M, Salmena L*, et al.* In Vivo Role of INPP4B in Tumor and Metastasis Suppression through Regulation of PI3K-AKT Signaling at Endosomes. Cancer Discov **2015**;5(7):740-51 doi 10.1158/2159-8290.CD-14-1347.

29. Liu SL, Wang ZG, Hu Y, Xin Y, Singaram I, Gorai S*, et al.* Quantitative Lipid Imaging Reveals a New Signaling Function of Phosphatidylinositol-3,4-Bisphophate: Isoform- and Site-Specific Activation of Akt. Mol Cell **2018**;71(6):1092-104 e5 doi 10.1016/j.molcel.2018.07.035.

30. Carver BS, Chapinski C, Wongvipat J, Hieronymus H, Chen Y, Chandarlapaty S*, et al.* Reciprocal feedback regulation of PI3K and androgen receptor signaling in PTEN-deficient prostate cancer. Cancer Cell **2011**;19(5):575-86 doi 10.1016/j.ccr.2011.04.008.

31. Mulholland DJ, Tran LM, Li Y, Cai H, Morim A, Wang S*, et al.* Cell autonomous role of PTEN in regulating castration-resistant prostate cancer growth. Cancer Cell **2011**;19(6):792-804 doi 10.1016/j.ccr.2011.05.006.

32. Hodgson MC, Shao LJ, Frolov A, Li R, Peterson LE, Ayala G*, et al.* Decreased expression and androgen regulation of the tumor suppressor gene INPP4B in prostate cancer. Cancer Res **2011**;71(2):572-82 doi 10.1158/0008-5472.CAN-10-2314.

33. Sweeney C, Bracarda S, Sternberg CN, Chi KN, Olmos D, Sandhu S*, et al.* Ipatasertib plus abiraterone and prednisolone in metastatic castration-resistant prostate cancer (IPATential150): a multicentre, randomised, double-blind, phase 3 trial. Lancet **2021**;398(10295):131-42 doi 10.1016/S0140-6736(21)00580-8.

34. Wang H, Xu Y, Fang Z, Chen S, Balk SP, Yuan X. Doxycycline regulated induction of AKT in murine prostate drives proliferation independently of p27 cyclin dependent kinase inhibitor downregulation. PLoS One **2012**;7(7):e41330 doi 10.1371/journal.pone.0041330.

35. Dong X, Xue H, Mo F, Lin YY, Lin D, Wong NKY*, et al.* Modeling Androgen Deprivation Therapy-Induced Prostate Cancer Dormancy and Its Clinical Implications. Mol Cancer Res **2022**;20(5):782-93 doi 10.1158/1541-7786.MCR-21-1037.

36. McKay RR, Xie W, Ye H, Fennessy FM, Zhang Z, Lis R*, et al.* Results of a Randomized Phase II Trial of Intense Androgen Deprivation Therapy prior to Radical Prostatectomy in Men with High-Risk Localized Prostate Cancer. J Urol **2021**;206(1):80-7 doi 10.1097/JU.0000000000001702.

37. Malek M, Kielkowska A, Chessa T, Anderson KE, Barneda D, Pir P*, et al.* PTEN Regulates PI(3,4)P(2) Signaling Downstream of Class I PI3K. Mol Cell **2017**;68(3):566-80 e10 doi 10.1016/j.molcel.2017.09.024.

38. Rodgers SJ, Ooms LM, Oorschot VMJ, Schittenhelm RB, Nguyen EV, Hamila SA*, et al.* INPP4B promotes PI3Kalpha-dependent late endosome formation and Wnt/beta-catenin signaling in breast cancer. Nat Commun **2021**;12(1):3140 doi 10.1038/s41467-021-23241-6.

39. Saffi GT, Wang CA, Mangialardi EM, Vacher J, Botelho RJ, Salmena L. Inhibition of lipid kinase PIKfyve reveals a role for phosphatase Inpp4b in the regulation of PI(3)P-mediated lysosome dynamics through VPS34 activity. J Biol Chem **2022**;298(8):102187 doi 10.1016/j.jbc.2022.102187.

40. Corey E, Quinn JE, Buhler KR, Nelson PS, Macoska JA, True LD*, et al.* LuCaP 35: a new model of prostate cancer progression to androgen independence. Prostate **2003**;55(4):239-46 doi 10.1002/pros.10198.

41. Cerami E, Gao J, Dogrusoz U, Gross BE, Sumer SO, Aksoy BA*, et al.* The cBio cancer genomics portal: an open platform for exploring multidimensional cancer genomics data. Cancer Discov **2012**;2(5):401-4 doi 10.1158/2159-8290.CD-12-0095.

42. Gao J, Aksoy BA, Dogrusoz U, Dresdner G, Gross B, Sumer SO*, et al.* Integrative analysis of complex cancer genomics and clinical profiles using the cBioPortal. Sci Signal **2013**;6(269):pl1 doi 10.1126/scisignal.2004088.

Figure Legends

Figure 1. INPP4B mRNA is negatively correlated with *T:E* fusion independently of *PTEN* status. (A) Correlation between ERG and PTEN mRNA in TCGA primary PCa. **(B)** Correlation between ERG and INPP4B mRNA in TCGA primary PCa. **(C)** Correlation between ERG and INPP4B mRNA, and *PTEN* genomic alterations, in TCGA primary PCa. **(D)** Correlation between PTEN and INPP4B mRNA, and PTEN genomic alterations, in TCGA primary PCa. **(E)** Correlation between ERG and IRS2 mRNA in TCGA primary PCa. All analyses were done on cBioPortal.

Figure 2. ERG suppresses AKT activity and IRS2 expression in PCA cells. (A) VCaP cells stably expressing an ERG shRNA versus a nontargeting control shRNA were assessed by immunoblotting as indicated. **(B)** VCaP cells were treated for 2 days with siRNA targeting ERG or a nontargeted control and assessed by immunoblotting as indicated. **(C)** LNCaP cells stably expressing a DOX-inducible HA-tagged ERG were treated with DOX over a time course and assessed by immunoblotting as indicated. **(D)** VCaP cells were treated for 2 days with siRNA targeting ERG or nontargeted control and assessed by immunoblotting as indicated.

Figure 3. PCa development in probasin-rtTA; tetO-ERG; *Pten*$^{-/+}$ mice. (A) Histology in mice treated for 1 – 11 months with DOX, showing foci of PCA in mouse treated with DOX for 11 months. **(B)** FFPE sections from representative areas with or without tumor were stained for ERG or the HA tag on ERG. Lower ERG expression is seen in areas with invasive tumor versus areas showing only dysplasia. **(C)** Higher pAKT and pS6 in areas with invasive tumor versus areas showing only dysplasia.

Figure 4. H19 lncRNA regulation by ERG in mouse model and human PCa. (A) H19 and IGF2 expression in mice with long-term DOX induction versus after DOX withdrawal. **(B)** H19, IGF2, and ERG expression in mouse prostate expressing probasin-ERG transgenes versus wild-type (from reference 13). **(C)** Correlation between ERG and H19 mRNA in TCGA primary PCa. **(D)** Correlation between ERG and H19 mRNA in *T:E* fusion positive tumors in TCGA primary PCa. **(E)** Correlation between ERG and H19 mRNA in *T:E* fusion negative tumors in TCGA primary PCa. Correlations were assessed in cBioPortal.

Figure 5. Androgen deprivation increases AKT activity and dependence in *T:E* fusion positive PDX. (A) *T:E* fusion positive BIDPC4 PDXs were established in male *scid* mice as subcutaneous tumors. Mice were sacrificed prior to or at ~2 weeks post-castration. FFPE sections were stained for ERG, pAKT(473), and pS6 as indicated, and representative slides are shown. (B) Cells from BIDPC4 PDX were cultured in medium with 10% FBS (FBS) or in medium with 10% charcoal stripped FBS (CSS). Ipatasertib was then added at the indicated concentrations and cell recovery was assessed by Cell Titer Glo assay after 7 days. Luminescent readouts were normalized to the average luminescent signal of DMSO under the respective conditions, with 6 replicates per dose of drug. The graph illustrates the half-maximal inhibitory concentration (IC50) in the presence of FBS

compared to CCS. Nonlinear regression curves were generated by a variable slope model. **(C)** Responses to MK2206 were assayed as in (B).

Figure 6. Castration increases AKT activity in additional *T:E* fusion positive versus negative PDXs. (A) *T:E* fusion positive LuCaP35 PDX were established and mice were sacrificed prior to castration of at 2 – 8 weeks after castration. FFPE sections were stained for pAKT or pS6, and representative sections are shown. **(B)** *T:E* fusion positive LTL310 xenografts were established under the kidney capsules in immunodeficient male mice,which were then sacrificed prior to castration, at 3 weeks after castration, or when tumors progressed after castration (resistant). FFPE sections were stained for pAKT or pS6, and representative sections are shown. **(C)** *T:E* fusion negative LTL607 PDXs were generated and analyzed as in (B).

Figure 7. AKT activity prior to and post-neoadjuvant intensive AR targeted therapy. (A) FFPE sections of tumor in pretreatment biopsies and in radical prostatectomy specimens from a *T:E* fusion positive and negative case were stained for pAKT(473). Samples were scored based on fraction of cells staining. Pretreatment biopsy scores for the *T:E* fusion positive and negative tumors shown here were 0 and 3, respectively. Scores for the corresponding post-treatment tumors were 3 (*T:E* fusion positive) and 2 (*T:E* fusion negative). **(B)** pAKT scores for each pre-treatment and corresponding post-treatment tumor in *T:E* fusion positive (left panel) and negative (right panel) cases. Note that darker lines reflect multiple cases with the same pre- and post-treatment scores. **(C)** For each patient the pAKT score in the pretreatment biopsy was subtracted from the score in the corresponding post-treatment tumor to give a differential pAKT score. The difference between the *T:E* fusion positive versus negative cases was significant ($p < .01$).

Figure 1

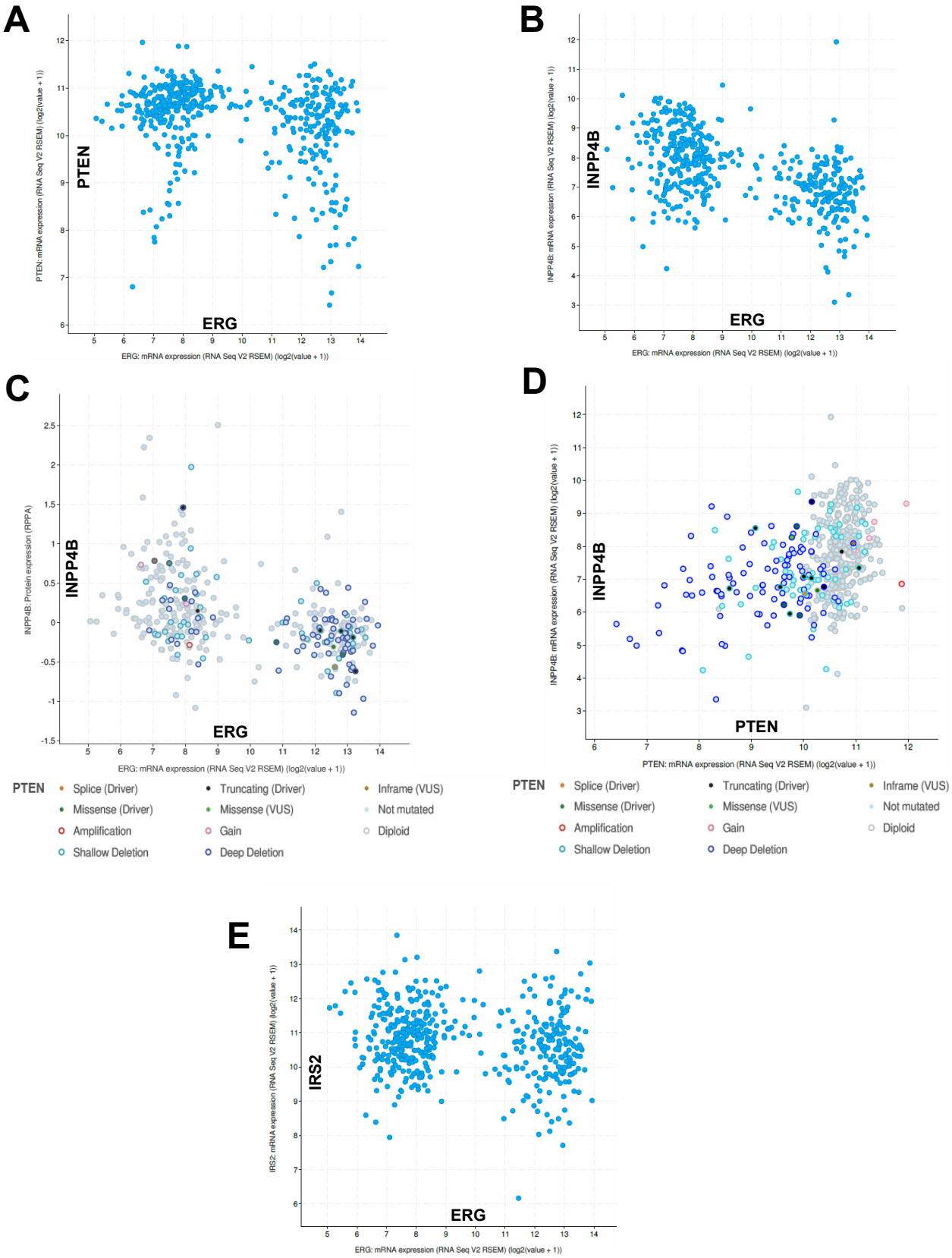
A
PTEN
ERG
PTEN: mRNA expression (RNA Seq V2 RSEM) (log2(value + 1))
ERG: mRNA expression (RNA Seq V2 RSEM) (log2(value + 1))
B
INPP4B
ERG
INPP4B: mRNA expression (RNA Seq V2 RSEM) (log2(value + 1))
ERG: mRNA expression (RNA Seq V2 RSEM) (log2(value + 1))
C
INPP4B
ERG
INPP4B: Protein expression (RPPA)
ERG: mRNA expression (RNA Seq V2 RSEM) (log2(value + 1))
D
INPP4B
PTEN
INPP4B: mRNA expression (RNA Seq V2 RSEM) (log2(value + 1))
PTEN: mRNA expression (RNA Seq V2 RSEM) (log2(value + 1))
PTEN
Splice (Driver)
Truncating (Driver)
Inframe (VUS)
Missense (Driver)
Missense (VUS)
Not mutated
Amplification
Gain
Diploid
Shallow Deletion
Deep Deletion
E
IRS2
ERG
IRS2: mRNA expression (RNA Seq V2 RSEM) (log2(value + 1))
ERG: mRNA expression (RNA Seq V2 RSEM) (log2(value + 1))

Figure 2

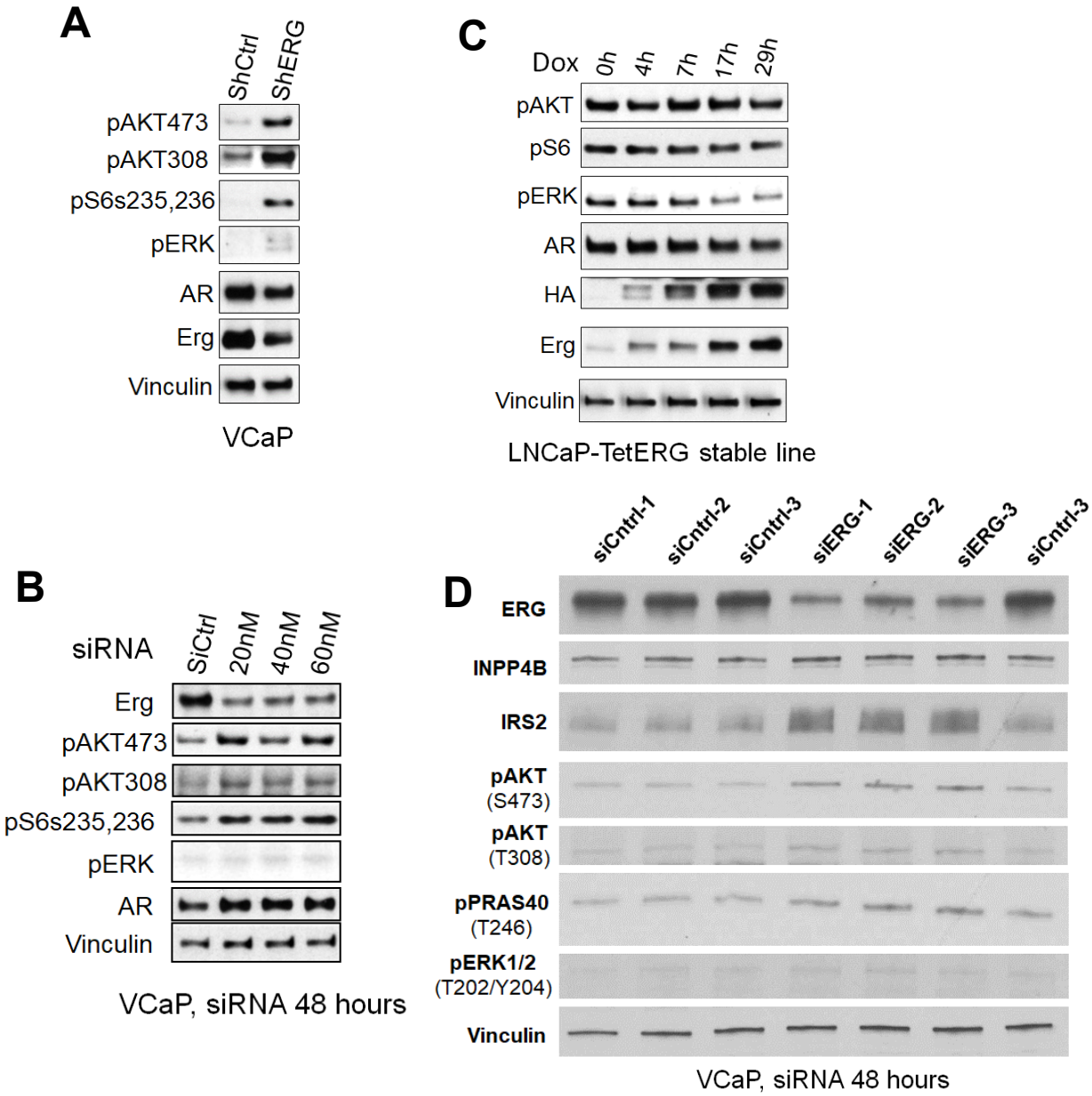
A
ShCtrl
ShERG
pAKT473
pAKT308
pS6s235,236
pERK
AR
Erg
Vinculin
VCaP
C
Dox
0h
4h
7h
17h
29h
pAKT
pS6
pERK
AR
HA
Erg
Vinculin
LNCaP-TetERG stable line
B
siRNA
SiCtrl
20nM
40nM
60nM
Erg
pAKT473
pAKT308
pS6s235,236
pERK
AR
Vinculin
VCaP, siRNA 48 hours
D
siCntrl-1
siCntrl-2
siCntrl-3
siERG-1
siERG-2
siERG-3
siCntrl-3
ERG
INPP4B
IRS2
pAKT (S473)
pAKT (T308)
pPRAS40 (T246)
pERK1/2 (T202/Y204)
Vinculin
VCaP, siRNA 48 hours

Figure 3

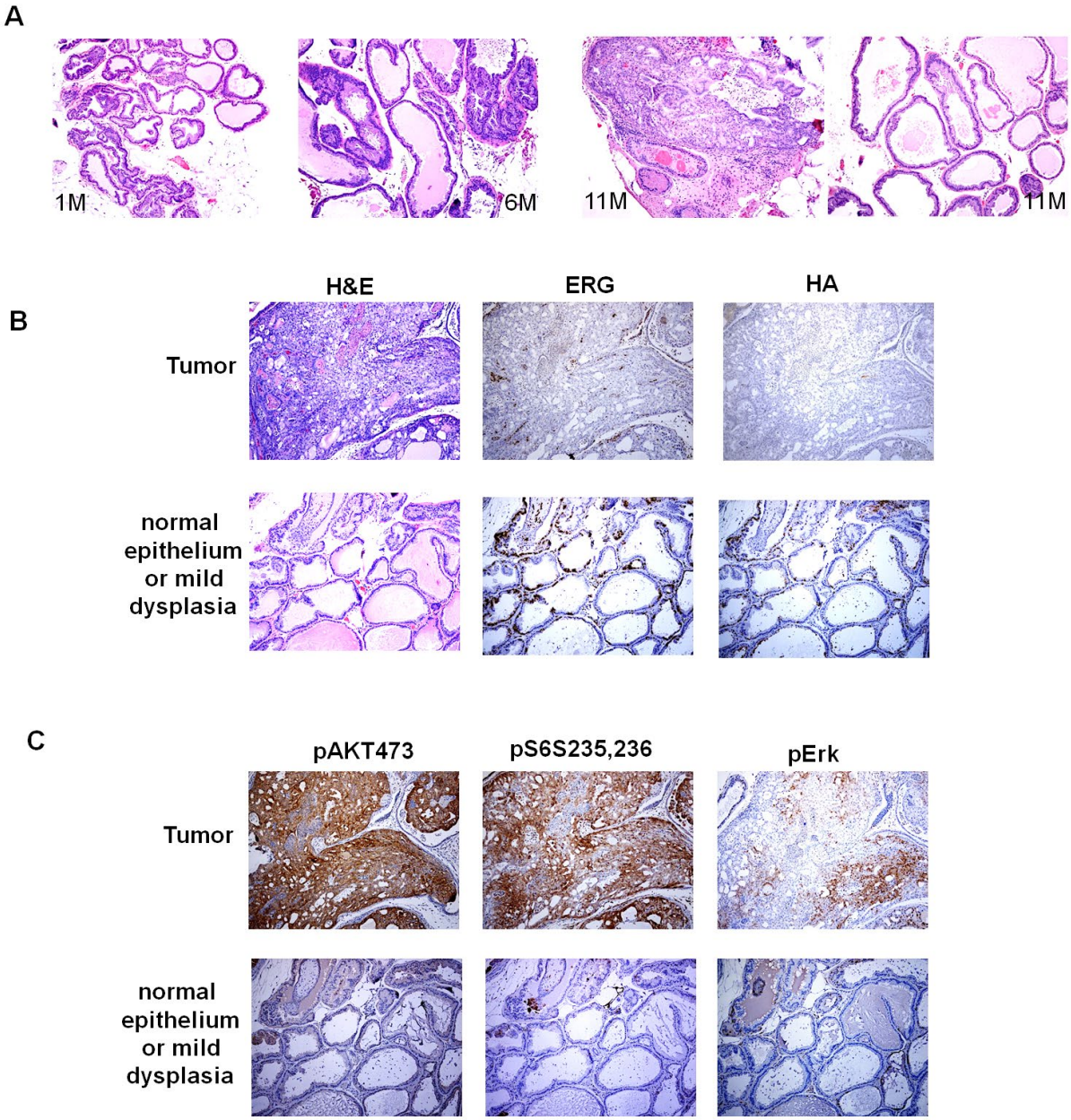
A
1M
6M
11M
11M
B
H&E
ERG
HA
Tumor
normal epithelium or mild dysplasia
C
pAKT473
pS6S235,236
pErk
Tumor
normal epithelium or mild dysplasia

Figure 4

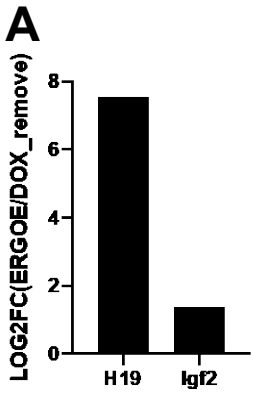
A
LOG2FC(ERGOE/DOX_remove)
0
2
4
6
8
H19
Igf2

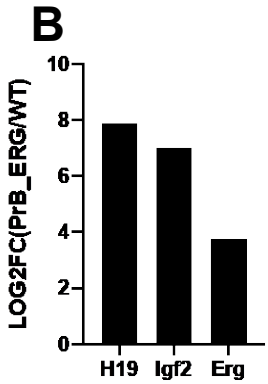
B
LOG2FC(PrB_ERG/WT)
0
2
4
6
8
10
H19
Igf2
Erg

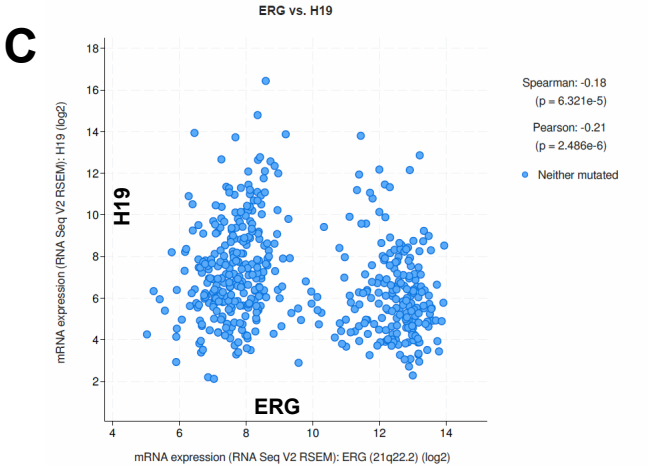
C
ERG vs. H19
Spearman: -0.18
(p = 6.321e-5)
Pearson: -0.21
(p = 2.486e-6)
Neither mutated
H19
ERG
mRNA expression (RNA Seq V2 RSEM): H19 (log2)
mRNA expression (RNA Seq V2 RSEM): ERG (21q22.2) (log2)

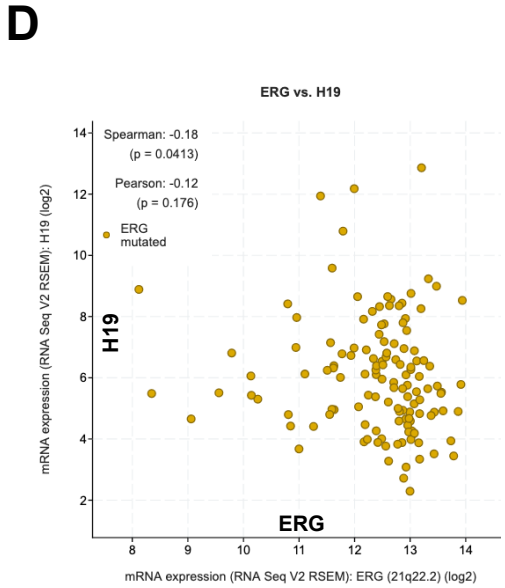
D
ERG vs. H19
Spearman: -0.18
(p = 0.0413)
Pearson: -0.12
(p = 0.176)
ERG
mutated
H19
ERG
mRNA expression (RNA Seq V2 RSEM): H19 (log2)
mRNA expression (RNA Seq V2 RSEM): ERG (21q22.2) (log2)

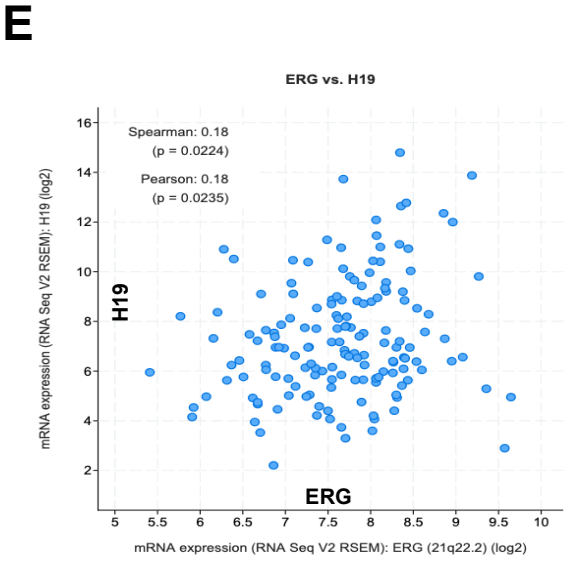
E
ERG vs. H19
Spearman: 0.18
(p = 0.0224)
Pearson: 0.18
(p = 0.0235)
H19
ERG
mRNA expression (RNA Seq V2 RSEM): H19 (log2)
mRNA expression (RNA Seq V2 RSEM): ERG (21q22.2) (log2)

Figure 5

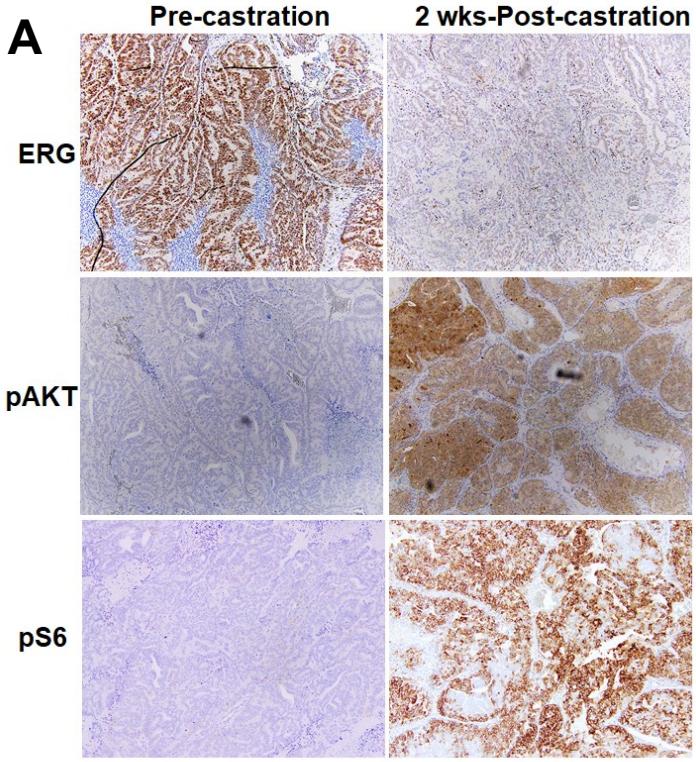

PC4-T:E positive

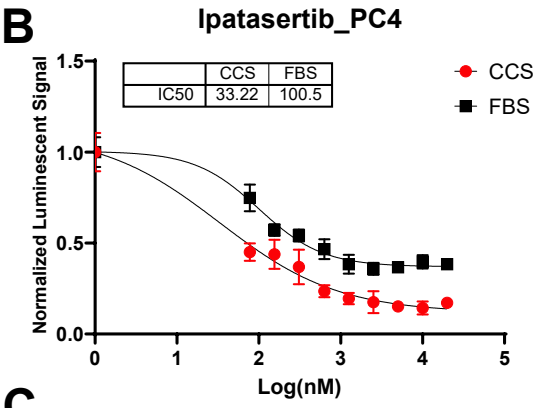

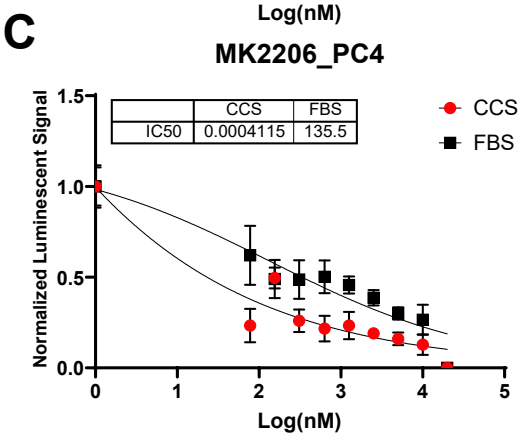

Figure 6

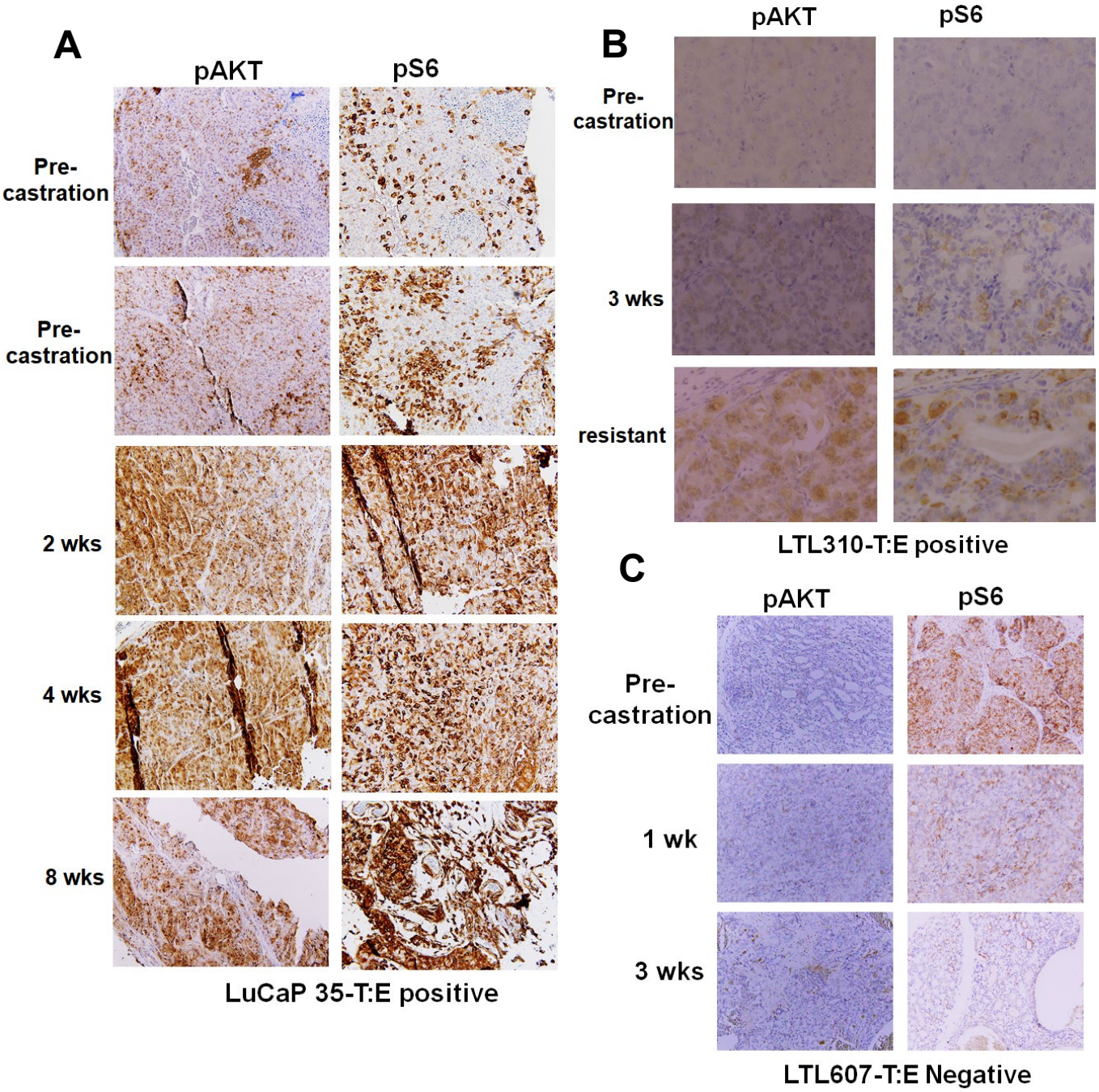
A
pAKT
pS6
Pre-castration
Pre-castration
2 wks
4 wks
8 wks
LuCaP 35-T:E positive
B
pAKT
pS6
Pre-castration
3 wks
resistant
LTL310-T:E positive
C
pAKT
pS6
Pre-castration
1 wk
3 wks
LTL607-T:E Negative

Figure 7

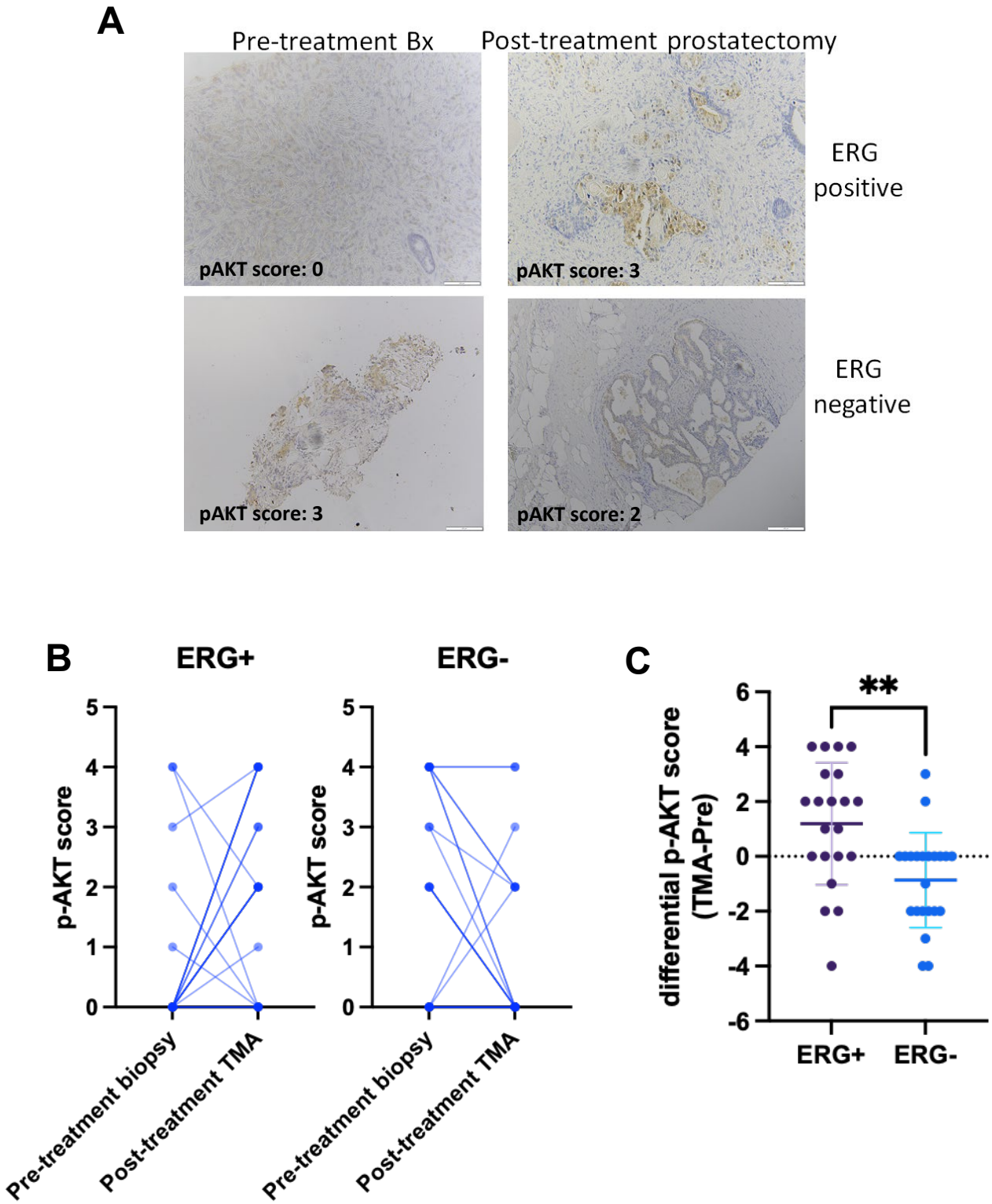
A
Pre-treatment Bx
Post-treatment prostatectomy
ERG positive
ERG negative
pAKT score: 0
pAKT score: 3
pAKT score: 3
pAKT score: 2
B
ERG+
ERG-
p-AKT score
0
1
2
3
4
5
Pre-treatment biopsy
Post-treatment TMA
C
differential p-AKT score (TMA-Pre)
6
4
2
0
-2
-4
-6
**
ERG+
ERG-